Journal of Quantitative Spectroscopy & Radiative Transfer 156 (2015) 97–108

Contents lists available at ScienceDirect

Journal of Quantitative Spectroscopy & Radiative Transfer

journal homepage: www.elsevier.com/locate/jqsrt

Polarized bidirectional reflectance of optically thick sparse particulate layers: An efficient numerically exact radiative-transfer solution

Michael I. Mishchenko [a,*], Janna M. Dlugach [b], Jacek Chowdhary [c], Nadezhda T. Zakharova [d]

[a] NASA Goddard Institute for Space Studies, 2880 Broadway, New York, NY 10025, USA
[b] Main Astronomical Observatory of the National Academy of Sciences of Ukraine, 27 Zabolotny Street, 03680 Kyiv, Ukraine
[c] Columbia University and NASA Goddard Institute for Space Studies, 2880 Broadway, New York, NY 10025, USA
[d] Trinnovim LLC, 2880 Broadway, New York, NY 10025, USA

ARTICLE INFO

Article history:
Received 10 November 2014
Received in revised form
31 January 2015
Accepted 3 February 2015
Available online 11 February 2015

Keywords:
Particulate media
Polarization
Electromagnetic scattering
Radiative transfer
Stokes parameters
Ambartsumian's nonlinear integral equation
Benchmark results

ABSTRACT

We describe a simple yet efficient numerical algorithm for computing polarized bidirectional reflectance of an optically thick (semi-infinite), macroscopically flat layer composed of statistically isotropic and mirror symmetric random particles. The spatial distribution of the particles is assumed to be sparse, random, and statistically uniform. The 4×4 Stokes reflection matrix is calculated by iterating the Ambartsumian's vector nonlinear integral equation. The result is a numerically exact solution of the vector radiative transfer equation and as such fully satisfies the energy conservation law and the fundamental reciprocity relation. Since this technique bypasses the computation of the internal radiation field, it is very fast and highly accurate. The FORTRAN implementation of the technique is publicly available on the World Wide Web at http://www.giss.nasa.gov/staff/mmishchenko/brf. It can be combined with several existing computer programs providing the requisite single-scattering properties of spherical or morphologically complex particles and applied to a wide range of optical characterization problems. Benchmark results obtained with this program can be used for testing alternative solvers of the vector radiative transfer equation.

Published by Elsevier Ltd.

1. Introduction

In a 1999 paper [1], we described an efficient numerical solution of the Ambartsumian's nonlinear integral equation satisfied by the reflection function of an optically semi-infinite, homogeneous layer of sparse discrete random medium. The corresponding FORTRAN implementation of this solution [2] has been used extensively by the research community to compute the bidirectional reflection function of optically thick particulate layers. The obvious limitation of the computer program [2] is its reliance on the scalar approximation [3] and the resulting inability to compute the polarized bidirectional reflection function. Therefore, the main objective of this paper is to describe in detail a natural extension of Ref. [1] wherein the scalar nonlinear integral equation is replaced by its full vector version as well as to serve as a step-by-step user guide to the corresponding computer programs. While the amount of new science in this user guide (similar in style to Refs. [4–11]) is by definition limited, the development of

* Corresponding author. Fax: +1 212 678 5622.
E-mail addresses: michael.i.mishchenko@nasa.gov, crmim2@gmail.com (M.I. Mishchenko).

http://dx.doi.org/10.1016/j.jqsrt.2015.02.003
0022-4073/Published by Elsevier Ltd.

a numerical algorithm that is both straightforward, user-friendly, and robust is always non-trivial and deserves a thorough discussion. We expect that the resulting computer programs [2] will be used both as an efficient analysis tool and as a source of benchmark numerical results suitable for testing alternative computer solvers of the vector radiative transfer equation.

To make the discussion in this paper more compact, we will use throughout the terminology and notation adopted in the monographs [3,12,13]. Note that Refs. [3,12] are available on-line as PDF files at http://www.giss.nasa.gov/staff/mmishchenko/books.html as well as at https://www.researchgate.net/profile/Michael_Mishchenko.

2. Vector nonlinear integral equation

Let us consider a semi-infinite, plane-parallel, statistically uniform layer of sparse discrete random medium extending in the vertical direction from $z=0$ to $z=-\infty$, where the z-axis of the laboratory right-handed coordinate system is perpendicular to the boundary of the medium and is directed upwards (Fig. 1). This implies that the particles constituting the layer are imbedded only in the lower half of the infinite homogeneous host medium. The host medium is assumed to be nonabsorbing.

A propagation direction $\hat{\mathbf{n}}$ at a point in space will be specified by a couplet $\{u,\varphi\}$, where $u=-\cos\theta\in[-1,+1]$ is the direction cosine, while θ and φ are the corresponding polar and azimuth angles with respect to the local coordinate system having the same spatial orientation as the laboratory coordinate system (Fig. 1). As usual, the polar (zenith) angle $\theta\in[0,\pi]$ is measured from the positive z-axis and the azimuth angle $\varphi\in[0,2\pi)$ is measured from the positive x-axis in the clockwise direction when looking in the direction of the positive z-axis. A positive u always corresponds to a downward direction, whereas a negative u always corresponds to an upward direction. It is also convenient to introduce a nonnegative quantity $\mu=|u|\in[0,1]$.

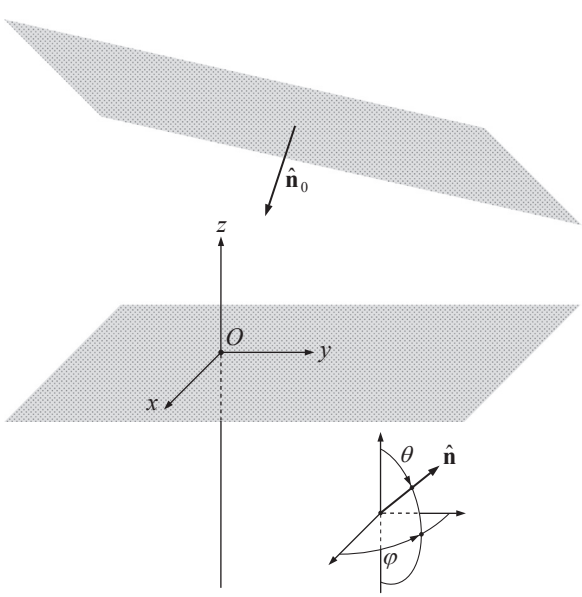

Fig. 1. Spherical coordinates used to specify the direction of light propagation.

The random particulate layer is illuminated from above by a plane electromagnetic wave or a parallel quasi-monochromatic beam of light propagating in the direction $\hat{\mathbf{n}}_0=\{u_0,\varphi_0\}=\{\mu_0,\varphi_0\}$. The uniformity and infinite transverse extent of the wave or the beam combined with the statistical uniformity of the particulate layer ensure that all parameters of the diffuse radiation field are independent of the coordinates x and y.

We assume the $\exp(-i\omega t)$ time-harmonic dependence of the electromagnetic field, where t is the time, ω is the angular frequency, and $i=(-1)^{1/2}$. This assumption implies a non-negative imaginary part of the particle relative refractive index. In accordance with Refs. [3,12,13], the four-component Stokes column vector of the incident light is defined as

$$\mathbf{I}_0=\begin{bmatrix} I_0\\ Q_0\\ U_0\\ V_0\end{bmatrix}=\frac{1}{2}\sqrt{\frac{\varepsilon_1}{\mu_0}}\begin{bmatrix}\langle\langle E_{0\theta}E_{0\theta}^*+E_{0\varphi}E_{0\varphi}^*\rangle\rangle\\ \langle\langle E_{0\theta}E_{0\theta}^*-E_{0\varphi}E_{0\varphi}^*\rangle\rangle\\ \langle\langle -E_{0\theta}E_{0\varphi}^*-E_{0\varphi}E_{0\theta}^*\rangle\rangle\\ i\langle\langle E_{0\varphi}E_{0\theta}^*-E_{0\theta}E_{0\varphi}^*\rangle\rangle\end{bmatrix}, \tag{1}$$

where ε_1 is the real-valued electric permittivity of the infinite host medium; μ_0 is the permeability of a vacuum (not to be confused with the direction cosine $\mu_0=u_0$); $\langle\langle\cdots\rangle\rangle$ denotes averaging over a "sufficiently long" period of time; $E_{0\theta}$ and $E_{0\varphi}$ are the θ- and φ-components of the electric field vector, respectively; and the asterisk denotes a complex-conjugate value. Note that the longitudinal component of the incident electric field is equal to zero since the electromagnetic field of the incident light is transverse. The same conventions as in Eq. (1) are used to define the 4-component diffuse specific intensity column vector $\tilde{\mathbf{I}}_{\rm d}(z,\hat{\mathbf{n}})=\tilde{\mathbf{I}}_{\rm d}(z,u,\varphi)$. The dimension of $\mathbf{I}_0$ is w m^{-2}, while that of $\tilde{\mathbf{I}}_{\rm d}$ is w m^{-2} sr^{-1}.

We assume that the random particles forming the scattering layer are statistically isotropic and mirror symmetric [3,13]. This allows one to fully characterize the optical properties of the particulate layer by the ensemble-averaged single-scattering albedo ϖ and so-called normalized 4×4 Stokes scattering matrix $\tilde{\mathbf{F}}(\Theta)$ with real-valued components. The latter has the well-known block-diagonal structure:

$$\tilde{\mathbf{F}}(\Theta)=\begin{bmatrix} a_1(\Theta) & b_1(\Theta) & 0 & 0\\ b_1(\Theta) & a_2(\Theta) & 0 & 0\\ 0 & 0 & a_3(\Theta) & b_2(\Theta)\\ 0 & 0 & -b_2(\Theta) & a_4(\Theta)\end{bmatrix}, \tag{2}$$

where $\Theta\in[0,\pi]$ is the angle between the incidence and scattering directions (i.e., the scattering angle). The (1,1) element (often called the phase function) is non-negative and satisfies the normalization condition:

$$\frac{1}{2}\int_0^\pi {\rm d}\Theta\,\sin\Theta a_1(\Theta)=1. \tag{3}$$

The assumption of low packing density of the particles forming the scattering slab allows one to compute the diffuse specific intensity column vector $\tilde{\mathbf{I}}_{\rm d}(z,\hat{\mathbf{n}})$ by solving

the standard vector radiative transfer equation [3,13]. However, the problem can be substantially simplified if one is interested only in radiometric and polarimetric characteristics of the "outgoing" diffuse light at the boundary of the slab, i.e., in the quantity $\tilde{\mathbf{I}}_{\rm d}(0,-\mu,\varphi)$. This happens, for example, when the detector of electromagnetic radiation (such as a well-collimated radiometer [13,14]) is placed outside the particulate medium. Indeed, then the linearity of the vector radiative transfer equation allows us to write

$$\tilde{\mathbf{I}}_{\rm d}(0,-\mu,\varphi)=\frac{1}{\pi}\mu_0\mathbf{R}(\mu,\varphi;\mu_0,\varphi_0)\mathbf{I}_0, \tag{4}$$

where $\mathbf{R}(\mu,\varphi;\mu_0,\varphi_0)$ is the 4×4 so-called reflection matrix with real-valued elements. This matrix satisfies the vector Ambartsumian's nonlinear integral equation

$$\begin{aligned}(\mu+\mu_0)\mathbf{R}(\mu,\varphi;\mu_0,\varphi_0)&=\frac{\varpi}{4}\tilde{\mathbf{Z}}(-\mu,\varphi;\mu_0,\varphi_0)\\&+\frac{\varpi\mu}{4\pi}\int_0^{2\pi}\mathrm{d}\varphi'\int_0^1\mathrm{d}\mu'\,\mathbf{R}(\mu,\varphi;\mu',\varphi')\tilde{\mathbf{Z}}(\mu',\varphi';\mu_0,\varphi_0)\\&+\frac{\varpi\mu_0}{4\pi}\int_0^{2\pi}\mathrm{d}\varphi'\int_0^1\mathrm{d}\mu'\,\tilde{\mathbf{Z}}(-\mu,\varphi;-\mu',\varphi')\mathbf{R}(\mu',\varphi';\mu_0,\varphi_0)\\&+\frac{\varpi\mu\mu_0}{4\pi^2}\int_0^{2\pi}\mathrm{d}\varphi'\int_0^1\mathrm{d}\mu'\int_0^{2\pi}\mathrm{d}\varphi''\int_0^1\mathrm{d}\mu''\\&\times\mathbf{R}(\mu,\varphi;\mu',\varphi')\tilde{\mathbf{Z}}(\mu',\varphi';-\mu'',\varphi'')\mathbf{R}(\mu'',\varphi'';\mu_0,\varphi_0)\end{aligned} \tag{5}$$

[3,15], in which the 4×4 real-valued matrix $\tilde{\mathbf{Z}}(u,\varphi;u',\varphi')$ is the so-called normalized phase matrix; its elements can be linearly expressed in terms of the elements of the normalized Stokes scattering matrix (2) (see, e.g., Section 11.10 of Ref. [3]). By solving Eq. (5), one completely bypasses the calculation of the internal radiation field, which helps make the corresponding numerical algorithm more computationally efficient and accurate.

In the rest of this paper we will discuss the numerical computation of the reflection matrix by solving the vector nonlinear integral equation (5) for a specific model of particles populating the semi-infinite scattering layer.

3. Fourier decomposition of the vector nonlinear integral equation

Although Eq. (5) can, in principle, be solved by iterations, the necessity of calculating four-fold integrals makes this solution quite time consuming. The calculation can be optimized by recognizing that the reflection matrix $\mathbf{R}(\mu,\varphi;\mu_0,\varphi_0)$ depends on the difference $\varphi-\varphi_0$ rather than on each azimuth angle separately and expanding $\mathbf{R}(\mu,\mu_0,\varphi-\varphi_0)$ in a Fourier series. An important preliminary step is to expand the elements of the normalized scattering matrix (2) in so-called generalized spherical functions $P^s_{mn}(\cos\Theta)$ [12,15]:

$$a_1(\Theta)=\sum_{s=0}^{s_{\max}}\alpha_1^sP^s_{00}(\cos\Theta), \tag{6}$$

$$a_2(\Theta)+a_3(\Theta)=\sum_{s=0}^{s_{\max}}(\alpha_2^s+\alpha_3^s)P^s_{22}(\cos\Theta), \tag{7}$$

$$a_2(\Theta)-a_3(\Theta)=\sum_{s=0}^{s_{\max}}(\alpha_2^s-\alpha_3^s)P^s_{2,-2}(\cos\Theta), \tag{8}$$

$$a_4(\Theta)=\sum_{s=0}^{s_{\max}}\alpha_4^sP^s_{00}(\cos\Theta), \tag{9}$$

$$b_1(\Theta)=\sum_{s=0}^{s_{\max}}\beta_1^sP^s_{02}(\cos\Theta), \tag{10}$$

$$b_2(\Theta)=\sum_{s=0}^{s_{\max}}\beta_2^sP^s_{02}(\cos\Theta), \tag{11}$$

where the upper summation limit $s_{\max}$ depends on the requisite numerical accuracy. Note that these expansions can also be written in terms of real-valued so-called Wigner d-functions:

$$d^s_{mn}(\Theta)=i^{n-m}P^s_{mn}(\cos\Theta) \tag{12}$$

(see Ref. [16] and Appendix F in Ref. [3]). One can then use the so-called addition theorem for the generalized spherical functions to show that the Fourier decomposition in azimuth of the reflection matrix has the following form [15,17,18]:

$$\begin{aligned}\mathbf{R}(\mu,\mu_0,\varphi-\varphi_0)&=\frac{1}{4}\sum_{m=0}^{m_{\max}}(2-\delta_{m0})\\&\times\{[(\mathbf{\Delta}+\mathbf{\Delta}_{34})\mathbf{R}^m(\mu,\mu_0)(\mathbf{\Delta}+\mathbf{\Delta}_{34})\\&+(\mathbf{\Delta}-\mathbf{\Delta}_{34})\mathbf{R}^m(\mu,\mu_0)(\mathbf{\Delta}-\mathbf{\Delta}_{34})]\,\cos m(\varphi-\varphi_0)\\&+[(\mathbf{\Delta}-\mathbf{\Delta}_{34})\mathbf{R}^m(\mu,\mu_0)(\mathbf{\Delta}+\mathbf{\Delta}_{34})\\&-(\mathbf{\Delta}+\mathbf{\Delta}_{34})\mathbf{R}^m(\mu,\mu_0)(\mathbf{\Delta}-\mathbf{\Delta}_{34})]\,\sin m(\varphi-\varphi_0)\},\end{aligned} \tag{13}$$

where δ_{ij} is the Kronecker delta;

$$\mathbf{\Delta}=\begin{bmatrix}1&0&0&0\\0&1&0&0\\0&0&1&0\\0&0&0&1\end{bmatrix}; \tag{14}$$

$$\mathbf{\Delta}_{34}=\begin{bmatrix}1&0&0&0\\0&1&0&0\\0&0&-1&0\\0&0&0&-1\end{bmatrix}; \tag{15}$$

the upper summation limit $m_{\max}\le s_{\max}$ is defined by the requisite numerical accuracy of computations; and each matrix $\mathbf{R}^m(\mu,\mu_0)$ satisfies a separate nonlinear integral equation:

$$\begin{aligned}(\mu+\mu_0)\mathbf{R}^m(\mu,\mu_0)&=\frac{\varpi}{4}\tilde{\mathbf{Z}}^m(-\mu,\mu_0)\\&+\frac{\varpi\mu}{2}\int_0^1\mathrm{d}\mu'\mathbf{R}^m(\mu,\mu')\tilde{\mathbf{Z}}^m(\mu',\mu_0)\\&+\frac{\varpi\mu_0}{2}\int_0^1\mathrm{d}\mu'\,\tilde{\mathbf{Z}}^m(-\mu,-\mu')\mathbf{R}^m(\mu',\mu_0)\\&+\varpi\mu\mu_0\int_0^1\mathrm{d}\mu'\int_0^1\mathrm{d}\mu''\,\mathbf{R}^m(\mu,\mu')\tilde{\mathbf{Z}}^m(\mu',-\mu'')\mathbf{R}^m(\mu'',\mu_0).\end{aligned} \tag{16}$$

The Fourier components of the normalized phase matrix are given by

$$\tilde{\mathbf{Z}}^m(u,u') = (-1)^m \sum_{s=m}^{s_{\max}} \mathbf{P}^s_m(u)\mathbf{S}^s\mathbf{P}^s_m(u'), \quad u,u' \in [-1,1], \tag{17}$$

where

$$\mathbf{P}^s_m(u) = \begin{bmatrix} P^s_{m0}(u) & 0 & 0 & 0 \\ 0 & P^s_{m+}(u) & P^s_{m-}(u) & 0 \\ 0 & P^s_{m-}(u) & P^s_{m+}(u) & 0 \\ 0 & 0 & 0 & P^s_{m0}(u) \end{bmatrix}, \tag{18}$$

$$P^s_{m\pm}(u) = \frac{1}{2}\left[P^s_{m,-2}(u) \pm P^s_{m2}(u)\right], \tag{19}$$

and

$$\mathbf{S}^s = \begin{bmatrix} \alpha^s_1 & \beta^s_1 & 0 & 0 \\ \beta^s_1 & \alpha^s_2 & 0 & 0 \\ 0 & 0 & \alpha^s_3 & \beta^s_2 \\ 0 & 0 & -\beta^s_2 & \alpha^s_4 \end{bmatrix}. \tag{20}$$

For actual computer calculations, it is convenient to rewrite Eq. (13) in an explicit form, as follows:

$$\begin{aligned} \mathbf{R}(\mu,\mu_0,\varphi-\varphi_0) = & \sum_{m=0}^{m_{\max}} (2-\delta_{m0}) \\ & \times \left(\begin{bmatrix} R^m_{11}(\mu,\mu_0) & R^m_{12}(\mu,\mu_0) & 0 & 0 \\ R^m_{21}(\mu,\mu_0) & R^m_{22}(\mu,\mu_0) & 0 & 0 \\ 0 & 0 & R^m_{33}(\mu,\mu_0) & R^m_{34}(\mu,\mu_0) \\ 0 & 0 & R^m_{43}(\mu,\mu_0) & R^m_{44}(\mu,\mu_0) \end{bmatrix} \cos m(\varphi-\varphi_0) \right. \\ & \left. + \begin{bmatrix} 0 & 0 & -R^m_{13}(\mu,\mu_0) & -R^m_{14}(\mu,\mu_0) \\ 0 & 0 & -R^m_{23}(\mu,\mu_0) & -R^m_{24}(\mu,\mu_0) \\ R^m_{31}(\mu,\mu_0) & R^m_{32}(\mu,\mu_0) & 0 & 0 \\ R^m_{41}(\mu,\mu_0) & R^m_{42}(\mu,\mu_0) & 0 & 0 \end{bmatrix} \sin m(\varphi-\varphi_0) \right). \end{aligned} \tag{21}$$

An important property of the azimuthal components of the reflection matrix is the symmetry relation

$$\mathbf{R}^m(\mu,\mu_0) = \mathbf{\Delta}_3[\mathbf{R}^m(\mu_0,\mu)]^{\mathrm{T}}\mathbf{\Delta}_3, \tag{22}$$

where T stands for "transposed" and

$$\mathbf{\Delta}_3 = \begin{bmatrix} 1 & 0 & 0 & 0 \\ 0 & 1 & 0 & 0 \\ 0 & 0 & -1 & 0 \\ 0 & 0 & 0 & 1 \end{bmatrix}. \tag{23}$$

By default, $n_{\max} = s_{\max}$. However, significantly smaller values may be sufficient depending on the actual illumination–reflection geometry. For example, only one (with $m=0$) or two (with $m=0$ and 2) Fourier terms are required in the case of normal incidence and/or reflection [19].

4. Numerical aspects and computer codes

According to the preceding sections, the computer calculation of the reflection matrix $\mathbf{R}(\mu,\varphi;\mu_0,\varphi_0)$ consists of an iterative solution of Eq. (16) for $0 \le m \le m_{\max}$ followed by the use of Eq. (21). In this section we discuss numerical aspects and a FORTRAN implementation of the iterative solution of Eq. (16). The corresponding computer programs are openly available on-line [2].

4.1. Angular discretization of Eq. (16)

In order to become solvable on a computer, Eq. (16) needs to be discretized. Specifically, using a quadrature integration formula on the interval $\mu \in [0,1]$ with N_G division points μ_k and weights w_k, the nonlinear integral equation (16) is converted into a system of N_G^2 nonlinear algebraic equations

$$\begin{aligned} (\mu_k+\mu_l)\mathbf{R}^m(\mu_k,\mu_l) = & \frac{\varpi}{4}\tilde{\mathbf{Z}}^m(-\mu_k,\mu_l) \\ & + \frac{\varpi\mu_k}{2}\sum_{n=1}^{N_G} w_n\mathbf{R}^m(\mu_k,\mu_n)\tilde{\mathbf{Z}}^m(\mu_n,\mu_l) \\ & + \frac{\varpi\mu_l}{2}\sum_{n=1}^{N_G} w_n\tilde{\mathbf{Z}}^m(-\mu_k,-\mu_n)\mathbf{R}^m(\mu_n,\mu_l) \\ & + \varpi\mu_k\mu_l\sum_{n=1}^{N_G}\sum_{n'=1}^{N_G} w_n w_{n'}\mathbf{R}^m(\mu_k,\mu_n)\tilde{\mathbf{Z}}^m(\mu_n,-\mu_{n'})\mathbf{R}^m(\mu_{n'},\mu_l) \end{aligned} \tag{24}$$

for the N_G^2 unknown matrices $\mathbf{R}^m(\mu_k,\mu_l)$ with $1 \le k,l \le N_G$. The iterative solution of this system of equations yields the numerical values of the matrices $\mathbf{R}^m(\mu,\mu_0)$ at pairs of quadrature division points. To find the matrices $\mathbf{R}^m(\mu,\mu_0)$ for μ and/or μ_0 not coinciding with any of the quadrature division points, one needs to use an interpolation or extrapolation procedure.

As discussed in Section 3.5 of Ref. [1], the Gaussian quadrature formula [20] has the highest algebraic degree of precision (i.e., a formula with N_G nodes is exact for all polynomials of degree $2N_G-1$ and lower) and is widely used in radiative transfer calculations to numerically evaluate integrals on the interval [0, 1]. An obvious drawback of this quadrature is that the largest division point is always smaller than unity, and if the values of $\mathbf{R}^m(\mu,\mu_0)$ for normal incidence and/or reflection are required then one must use an extrapolation procedure. This often results in poor numerical accuracy and dictates the use of the Gaussian quadrature formula with an excessive number N_G of quadrature nodes. A more efficient approach is to use the so-called Markov quadrature formula [20] with one predefined node $\mu_{N_G}=1$. This formula still has the highest possible algebraic precision (i.e., is exact for all polynomials of degree $2N_G-2$ and lower) while eliminating the need for extrapolation to $\mu=1$ and/or $\mu_0=1$. Another efficient way of avoiding excessive N_G values in radiative transfer computations is to apply the Gaussian quadrature to the interval $[0,\pi/2]$ of $\arccos\mu$ values [1]. The respective division points and weights in Eq. (24) are given by

$$\mu_n = \cos\left(\frac{\pi}{4}X_n + \frac{\pi}{4}\right), \quad w_n = \frac{\pi}{4}W_n \sin\left(\frac{\pi}{4}X_n + \frac{\pi}{4}\right), \tag{25}$$

where X_n and W_n with $n=1, \ldots, N_G$ are the Gaussian nodes and weights, respectively, on the interval $[-1,1]$.

4.2. Fourier components of the phase matrix

The numerical solution of Eq. (24) must be preceded by the computation of the matrices $\tilde{\mathbf{Z}}^m(\pm\mu_k,\pm\mu_l)$ according to Eqs. (17)–(20) and, thus, by the computation of the coefficients entering the expansions (6)–(11). Fig. 2 shows

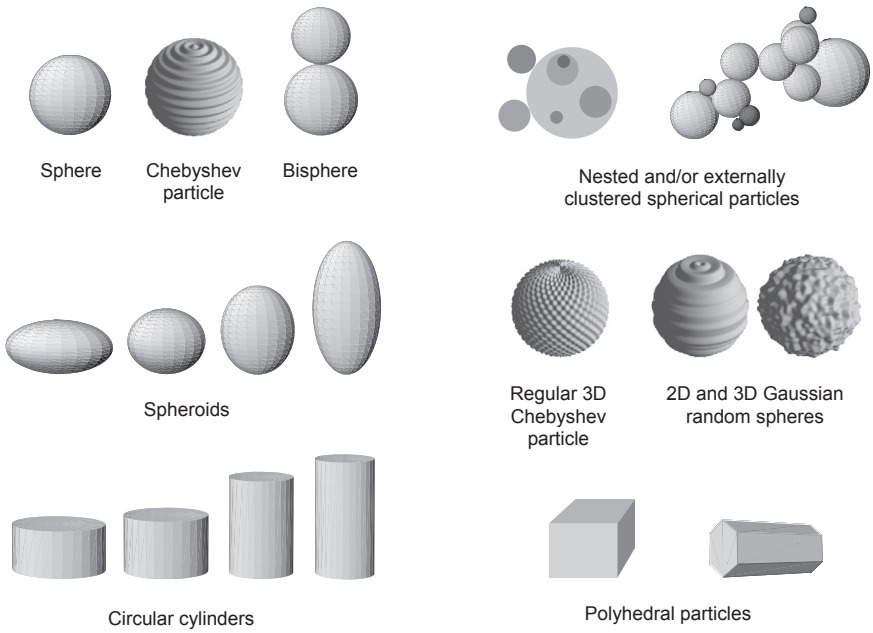

Fig. 2. Spherically symmetric and nonspherical particle morphologies.

examples of spherically symmetric and complex particle morphologies for which the α and β coefficients can be calculated numerically using the Lorenz–Mie theory or the (superposition) T-matrix method. In particular, the computations can be performed for

- monodisperse of polydisperse homogeneous spherical particles (Section 5.10 of Ref. [12]);
- monodisperse or polydisperse, randomly oriented homogeneous spheroids, circular cylinders, and Chebyshev particles (Ref. [4] or Section 5.11 of Ref. [12]);
- monodisperse bispheres [21];
- clusters of separated, externally touching, and/or nested spheres [7,22,23].

The corresponding FORTRAN computer programs are publicly available on-line [24]. Other nonspherical shapes shown in Fig. 2 can be handled using the T-matrix code described in Ref. [10] and also publicly available on-line [25].

To compute the generalized spherical functions entering Eqs. (18) and (19), we use Eq. (12) in combination with the following recurrence relation for the Wigner d-functions:

$$d_{mn}^{s+1}(\theta)=\frac{1}{s\sqrt{(s+1)^2-m^2}\sqrt{(s+1)^2-n^2}}\times\{(2s+1)[s(s+1)x-mn]d_{mn}^{s}(\theta)-(s+1)\sqrt{s^2-m^2}\sqrt{s^2-n^2}d_{mn}^{s-1}(\theta)\},\tag{26}$$

where $s \geq s_{\min}$ and

$$s_{\min}=\max(|m|,|n|).\tag{27}$$

Note that in general, $d_{mn}^{s}(\theta)\equiv 0$ for $s<s_{\min}$. The initial values for the recurrence relation (26) are given by

$$d_{mn}^{s_{\min}-1}(\theta)=0,\tag{28}$$

$$d_{mn}^{s_{\min}}(\theta)=\xi_{mn}2^{-s_{\min}}\left[\frac{(2s_{\min})!}{(|m-n|)!(|m+n|)!}\right]^{1/2}\times(1-x)^{|m-n|/2}(1+x)^{|m+n|/2},\tag{29}$$

where

$$\xi_{mn}=\begin{cases}1 & \text{for} \quad n\geq m,\\ (-1)^{m-n} & \text{for} \quad n<m.\end{cases}\tag{30}$$

Theoretically, the $(1,1)$ element of the zeroth component of the phase matrix must satisfy the normalization condition

$$\frac{1}{2}\int_{-1}^{1}\mathrm{d}u'\,\tilde{Z}_{11}^{0}(u,u')=1\tag{31}$$

for any u. However, the use of a quadrature formula in the actual numerical integration can yield u-dependent values deviating from unity, which can cause a significant violation of the energy conservation law [26,27]. To enforce the normalization (31), we use a numerical renormalization procedure described in Section 3.6 of Ref. [1].

4.3. Iterative solution of Eq. (24)

Eq. (24) is solved by iterations, i.e., the improved Lth approximation $[\mathbf{R}^m(\mu_k,\mu_l)]^L$ is obtained by substituting the previous approximation $[\mathbf{R}^m(\mu_k,\mu_l)]^{L-1}$ into the right-hand side:

$$[\mathbf{R}^m(\mu_k,\mu_l)]^L=\frac{1}{\mu_k+\mu_l}\left[\frac{\varpi}{4}\tilde{\mathbf{Z}}^m(-\mu_k,\mu_l)\right.$$

$$+\frac{\varpi\mu_k}{2}\sum_{n=1}^{N_G} w_n\left[\mathbf{R}^m(\mu_k,\mu_n)\right]^{L-1}\tilde{\mathbf{Z}}^m(\mu_n,\mu_l)$$
$$+\frac{\varpi\mu_l}{2}\sum_{n=1}^{N_G} w_n\tilde{\mathbf{Z}}^m(-\mu_k,-\mu_n)\left[\mathbf{R}^m(\mu_n,\mu_l)\right]^{L-1}$$
$$+\varpi\mu_k\mu_l\sum_{n=1}^{N_G}\sum_{n'=1}^{N_G} w_n w_{n'}\left[\mathbf{R}^m(\mu_k,\mu_n)\right]^{L-1}$$
$$\times\tilde{\mathbf{Z}}^m(\mu_n,-\mu_{n'})\left[\mathbf{R}^m(\mu_{n'},\mu_l)\right]^{L-1}\Big]. \tag{32}$$

The initial approximation is given by

$$[\mathbf{R}^m(\mu_k,\mu_l)]^0=\frac{\varpi}{4(\mu_k+\mu_l)}\tilde{\mathbf{Z}}^m(-\mu_k,\mu_l). \tag{33}$$

To reduce the computer time, the right-hand side of Eq. (32) is evaluated only for $l\le k$. The remaining matrices $[\mathbf{R}^m(\mu_k,\mu_l)]^L$ with $l>k$ are found from the reciprocity relation (22). The iterations stop when $[\mathbf{R}^m(\mu_k,\mu_l)]^L$ and $[\mathbf{R}^m(\mu_k,\mu_l)]^{L-1}$ differ (in the absolute-value sense) by less than a prescribed accuracy parameter:

$$\max_{\substack{1\le k,l\le N_G\\ 1\le p,q\le 4}}|[R^m_{pq}(\mu_k,\mu_l)]^L-[R^m_{pq}(\mu_k,\mu_l)]^{L-1}|\le\varepsilon. \tag{34}$$

For large values of m, the initial approximation (33) can already be sufficiently accurate so that no further iterations are needed. Numerical experiments have shown that this happens when

$$\left(\max_{m\le s\le s_{\max}}|\alpha_1^s|\right)\max_{m\le s\le s_{\max}}\left|\frac{\alpha_1^s}{2s+1}\right|\le\varepsilon. \tag{35}$$

Note that this criterion is less conservative than that suggested by de Rooij [17].

When $m=0$ and $\varpi=1$, the iterative process diverges owing to non-uniqueness of solutions of the nonlinear integral equation [28]. In this case we enforce convergence using the approach developed by de Rooij [17]. Furthermore, for $m\le 2$ and $\varpi\ge 0.8$, we accelerate convergence by using a linear improvement of the Lth approximation according to

$$[\mathbf{R}^m(\mu_k,\mu_l)]^{L,\text{improved}}=[\mathbf{R}^m(\mu_k,\mu_l)]^L+\gamma\{[\mathbf{R}^m(\mu_k,\mu_l)]^L$$
$$-[\mathbf{R}^m(\mu_k,\mu_l)]^{L-1}\}. \tag{36}$$

The default value of the coefficient γ is 0.8ϖ, although it is not inconceivable that in some cases it will need to be reduced to ensure convergence of the iterations. In all other cases even the simple iterations converge very fast and require no acceleration.

4.4. Supermatrices

Following Refs. [18,29], let us introduce the $KN_G\times KN_G$ so-called supermatrices

$$[\mathbf{R}^m]_{K(k-1)+p,K(l-1)+q}=\sqrt{w_k w_l}\,R^m_{pq}(\mu_k,\mu_l), \tag{37}$$

$$[\tilde{\mathbf{Z}}^m_{\pm\pm}]_{K(k-1)+p,K(l-1)+q}=\sqrt{w_k w_l}\,\tilde{Z}^m_{pq}(\pm\mu_k,\pm\mu_l), \tag{38}$$

$$[\mathbf{C}^m]_{K(k-1)+p,K(l-1)+q}=\mu_k\,\delta_{kl}\,\delta_{pq}, \tag{39}$$

where by default, $K=4$, $1\le k,l\le N_G$, and $1\le p,q\le K$. In other words, each supermatrix is an $N_G\times N_G$ array of $K\times K$ blocks. Then the nonlinear integral equation (24) can be re-written in a very compact supermatrix form:

$$\mathbf{C}\mathbf{R}^m+\mathbf{R}^m\mathbf{C}=\frac{\varpi}{4}\tilde{\mathbf{Z}}^m_{-+}+\frac{\varpi}{2}\mathbf{C}\mathbf{R}^m\tilde{\mathbf{Z}}^m_{++}$$
$$+\frac{\varpi}{2}\tilde{\mathbf{Z}}^m_{--}\mathbf{R}^m\mathbf{C}+\varpi\mathbf{C}\mathbf{R}^m\tilde{\mathbf{Z}}^m_{+-}\mathbf{R}^m\mathbf{C}. \tag{40}$$

As a result, each combination {matrix multiplication, μ-integration} has been replaced by a single matrix multiplication, which is highly advantageous for computational purposes.

4.5. Type of output and useful simplifications

The default value $K=4$ implies the computation of the full 4×4 reflection matrix. An important advantage of the supermatrix approach is that by specifying K values smaller than 4, one can easily implement three widely used simplifications and thereby reduce the computer time. First of all, it is well known that the zeroth component of the reflection matrix $\mathbf{R}^0(\mu,\mu_0)$ is block-diagonal, the upper right and lower left 2×2 submatrices being zero [17,29]. Therefore, if it is known beforehand that only the first two components of the Stokes column vector of the incident light (1) can be nonzero, then one can specify $K=2$ for $m=0$ without any loss of accuracy.

Second of all, let us assume that the incident light is unpolarized, while the 4th Stokes parameter of the reflected light is expected to be negligibly small and does not affect significantly the other Stokes parameters. This is the gist of the 3×3 approximation [26]. In this case one can specify $K=2$ for $m=0$ and $K=3$ for $m>0$.

Finally, by specifying $K=1$ for all m, one implements the scalar approximation. Now the underlying assumptions are that the incident light is unpolarized, only the first Stokes parameter (i.e., the specific intensity) of the reflected light is sought, and all elements of the scattering matrix but the $(1,1)$ element can be neglected without significant loss of accuracy in the computed intensity [3,30].

4.6. Computer programs

The computer solver of the nonlinear integral equation (5) is implemented in the form of the FORTRAN programs pbrf.f and pbrf.par.f. The latter includes the following user-specified input parameters:

- NG$=N_G$;
- NQUADR specifies the type of quadrature integration formula used: the special formula given by Eq. (25), the Gaussian formula, or the Markov formula;
- NCASE specifies the type of output in terms of the parameter KONTR$=K$ according to Section 4.5; and
- EP$=\varepsilon$ in Eq. (34).

The program pbrf.f also reads in the single-scattering albedo ALB$=\varpi$, the parameter LMAX1$=s_{\max}+1$, and the expansion coefficients entering Eqs. (6)–(11).

The output of the program pbrf.f consists of

- the parameter NG$=N_G$;
- the quadrature division points X(I)$=\mu_i$, $1\le$ I $\le$ NG;
- the parameter LMAX1$=s_{\max}+1$; and

- the sequentially stored converged values of the $s_{\max}+1$ Fourier components of the reflection matrix R(K,L,I,J)= $R^m_{kl}(\mu_i,\mu_j)$, $0 \le m \le s_{\max}$, $1 \le \mathrm{K,L} \le 4$, $1 \le \mathrm{I,J} \le \mathrm{NG}$.

Note that certain $R^m_{kl}(\mu_i,\mu_j)$ values can be zero depending on the output type specified by the parameter NCASE.

The program pbrf.f has been tested against numerical data documented in Table 4.18 of Ref. [17]. In all cases, our results agreed with those in Ref. [17] to within 2×10^{-5}. Note that the use of the $\exp(i\omega t)$ time-harmonic dependence of the electromagnetic field in Ref. [17] results in the opposite sign of the reflection matrix elements in the fourth row and the fourth column, except the R_{44} element.

5. Benchmark results

The actual numerical accuracy of the final output in terms of the matrices $\mathbf{R}^m(\mu,\mu_0)$ depends on many input-parameter choices that one needs to make in the computation of the single-scattering quantities entering Eq. (24) and then in the numerical solution of this equation. To generate benchmark results with a guaranteed number of exact decimals, all input parameters affecting the final numerical accuracy need to be appropriately varied until the results no longer change by more than a prescribed uncertainty. Importantly, this uncertainty is not necessarily equal to a formal accuracy parameter such as ε in Eq. (34). Indeed, if the convergence of the iterations is slow then two sequential iterations may differ by less than ε and yet deviate from the exact result by a much larger amount. Therefore, one may need to specify an ε value equal to one-tenth or one-hundredth of the requisite final uncertainty.

Benchmark numbers are invaluable in testing newly developed radiative-transfer software but are scarcely available. Therefore, below we present a set of benchmark values of the matrices $\mathbf{R}^m(\mu,\mu_0)$ and describe in detail how they have been generated.

Our model of the scattering object is a homogeneous semi-infinite slab composed of polydisperse, homogeneous, spherical particles representative of the cloud particles in the atmosphere of Venus [31]. Specifically, the relative refractive index of the particles is 1.44 and the dispersion of their radii is described by the gamma size distribution

$$n(r) = \text{constant} \times r^{(1-3b)/b} \exp\left(-\frac{r}{ab}\right), \quad r \in [r_{\min}, r_{\max}] \tag{41}$$

with $a=1.05$ μm, $b=0.07$, $r_{\min}=0$, and $r_{\max}=5$ μm. The constant is defined by the normalization condition

$$\int_{r_{\min}}^{r_{\max}} \mathrm{d}r\, n(r) = 1. \tag{42}$$

The effective radius and effective variance of a size distribution are defined as

$$r_{\text{eff}} = \frac{1}{\langle G\rangle}\int_{r_{\min}}^{r_{\max}} \mathrm{d}r\, n(r) r \pi r^2 \tag{43}$$

and

$$v_{\text{eff}} = \frac{1}{\langle G\rangle r_{\text{eff}}^2}\int_{r_{\min}}^{r_{\max}} \mathrm{d}r\, n(r)(r-r_{\text{eff}})^2 \pi r^2, \tag{44}$$

respectively, where

$$\langle G\rangle = \int_{r_{\min}}^{r_{\max}} \mathrm{d}r\, n(r)\pi r^2 \tag{45}$$

is the average area of the geometric projection per particle [32]. For the gamma size distribution considered, $r_{\text{eff}} = 1.0500000$ μm and $v_{\text{eff}} = 0.0700000$. In other words, the effective radius and effective variance essentially coincide with the parameters a and b, respectively, which implies that our "truncated" size distribution is virtually indistinguishable from that with $r_{\max}=\infty$. The wavelength of the incident light is set at 0.55 μm.

To generate the expansion coefficients entering Eqs. (6)–(11), we used the program spher.f [2] (see also Section 5.10 of Ref. [12]) with the following input parameters:

```
AA=1.05D0
BB=0.07D0
LAM=0.55D0
MRR=1.44D0
MRI=0D0
NDISTR=4
NK=600
N=500
R1=0D0
R2=5D0
DDELT=1D-7
```

In other words, the integration interval [0, 5] μm was subdivided into 500 equal subintervals, and a Gaussian integration formula with 600 division points was applied to each subinterval. Also, we kept only the expansion coefficients with an absolute value greater than or equal to 10^{-7}. The resulting output is partially illustrated by Table 1. By increasing N and NK, we have verified that the above input parameters guarantee the validity of all the digits given. The corresponding nonzero elements of the normalized scattering matrix (2) are listed in Table 2 and visualized in Fig. 3. Note that in the case of homogeneous spherical particles, $a_2(\Theta)\equiv a_1(\Theta)$ and $a_4(\Theta)\equiv a_3(\Theta)$. Again, the accuracy of all the numbers in Table 2 is expected to be better than one unit in the last decimals given. Since the imaginary part of the relative refractive index is zero, the extinction cross section $C_{\text{ext}} = 6.634121$ μm^2 is equal to the scattering cross section, while the single-scattering albedo is equal to unity.

We then used the program pbrf.f [2] to compute the Fourier components of the reflection matrix using the input parameters NCASE=4 and EP=1D–7. To tabulate maximally accurate results, we avoided the use of an interpolation procedure and calculated the matrices $\mathbf{R}^m(0.5,0.5)$ by using the Gaussian quadrature formula (NQUADR=2) with NG=49 division points, which ensured that the 25th division point μ_{25} was identically equal to 0.5 (this is true of the central quadrature point of the Gaussian quadrature formula with any odd NG). Similarly, we calculated the matrices $\mathbf{R}^m(1,1)$ by using the Markov

Table 1
Expansion coefficients.

s	α_1^s	α_2^s	α_3^s	α_4^s	β_1^s	β_2^s
0	1.0000000	0.0000000	0.0000000	0.8646237	0.0000000	0.0000000
1	2.1539916	0.0000000	0.0000000	2.2364652	0.0000000	0.0000000
2	3.1924464	4.0624621	3.7389742	3.0176502	−0.0635903	0.0993650
3	3.3489548	3.8176284	3.8851805	3.4284891	−0.0277256	−0.0302883
4	4.0711985	4.2722405	4.0656001	3.9144360	−0.0238844	0.0995472
5	4.2075358	4.3992879	4.4249308	4.2253032	0.0330322	−0.1742546
6	4.6650816	4.8255510	4.7450788	4.6272864	0.0487216	0.0998173
7	4.8580255	4.9521780	4.8726160	4.8099060	0.0213805	−0.2628473
8	5.0138968	5.2221526	5.2008052	5.0411050	0.0507196	0.0493398
9	5.1618856	5.1917857	5.0830935	5.1121738	−0.0170025	−0.3064218
10	5.0699649	5.3340874	5.3181143	5.1229466	0.0399854	−0.0289850
11	5.1251999	5.1101453	5.0071562	5.1085322	−0.0378515	−0.3204297
12	4.8590337	5.1661379	5.1236353	4.9101188	0.0151606	−0.1113303
13	4.8124876	4.7656681	4.6808215	4.8364599	−0.0458112	−0.3247146
14	4.4346709	4.7668527	4.6937932	4.4766728	−0.0136849	−0.1868049
15	4.2932504	4.2282350	4.1606320	4.3519012	−0.0442579	−0.3183069
…	…	…	…	…	…	…
61	0.0000196	0.0000184	0.0000174	0.0000220	−0.0000022	−0.0000024
62	0.0000319	0.0000357	0.0000194	0.0000182	0.0000001	−0.0000121
63	0.0000090	0.0000084	0.0000080	0.0000102	−0.0000011	−0.0000011
64	0.0000153	0.0000171	0.0000091	0.0000085	0.0000000	−0.0000057
65	0.0000041	0.0000038	0.0000036	0.0000047	−0.0000005	−0.0000005
66	0.0000073	0.0000081	0.0000042	0.0000039	0.0000000	−0.0000026
67	0.0000018	0.0000017	0.0000016	0.0000021	−0.0000002	−0.0000002
68	0.0000034	0.0000038	0.0000020	0.0000018	0.0000000	−0.0000012
69	0.0000008	0.0000008	0.0000007	0.0000010	−0.0000001	−0.0000001
70	0.0000016	0.0000018	0.0000009	0.0000008	0.0000000	−0.0000005
71	0.0000004	0.0000003	0.0000003	0.0000004	−0.0000001	−0.0000001
72	0.0000007	0.0000008	0.0000004	0.0000004	0.0000000	−0.0000002
73	0.0000002	0.0000001	0.0000001	0.0000002	0.0000000	0.0000000
74	0.0000003	0.0000004	0.0000002	0.0000002	0.0000000	−0.0000001
75	0.0000001	0.0000001	0.0000001	0.0000001	0.0000000	0.0000000

Table 2
Elements of the normalized scattering matrix.

Θ (deg.)	$a_1(\Theta)$	$a_3(\Theta)$	$b_1(\Theta)$	$b_2(\Theta)$
0	96.402333	96.402333	0.000000	0.000000
10	20.785319	20.349041	0.179854	1.647124
20	3.622231	3.442629	−0.098971	0.089643
30	2.068018	1.951312	−0.028020	−0.016245
40	1.308097	1.218481	0.033648	−0.055846
50	0.849585	0.769638	0.064140	−0.062030
60	0.555742	0.479211	0.067571	−0.059261
70	0.371607	0.292706	0.053323	−0.055422
80	0.257313	0.170601	0.034408	−0.049382
90	0.184696	0.090538	0.021518	−0.041143
100	0.137025	0.040962	0.016616	−0.033059
110	0.106302	0.012803	0.016565	−0.027428
120	0.090714	−0.001991	0.019198	−0.026973
130	0.096743	−0.009754	0.025391	−0.040007
140	0.151038	−0.017513	0.036702	−0.093368
150	0.300171	−0.040175	0.033705	−0.231587
160	0.629565	0.032510	−0.073537	−0.515500
170	0.698692	0.375344	−0.038232	−0.310203
180	0.708431	−0.708431	0.000000	0.000000

quadrature formula (NQUADR=3) with NG=50 division points, which ensured that the 50th division point μ_{50} was identically equal to unity. By increasing NG (while keeping it odd for the Gaussian quadrature formula) and decreasing EP, we have verified that these input parameters guaranteed all decimals in the benchmark numbers given below:

$$\mathbf{R}^0(0.5,0.5)=\begin{bmatrix} 1.054548 & -0.005217 & 0.000000 & 0.000000 \\ -0.005217 & 0.262763 & 0.000000 & 0.000000 \\ 0.000000 & 0.000000 & 0.146687 & 0.032284 \\ 0.000000 & 0.000000 & -0.032284 & 0.208790 \end{bmatrix}, \tag{46}$$

$$\mathbf{R}^1(0.5,0.5)=\begin{bmatrix} 0.039998 & 0.007864 & -0.014080 & -0.000034 \\ 0.007864 & 0.045349 & 0.035117 & -0.019115 \\ 0.014080 & -0.035117 & 0.164078 & -0.032249 \\ -0.000034 & -0.019115 & 0.032249 & 0.114666 \end{bmatrix}, \tag{47}$$

$$\mathbf{R}^2(0.5,0.5)=\begin{bmatrix} 0.087256 & 0.011310 & -0.008222 & 0.000056 \\ 0.011310 & 0.092563 & -0.027371 & -0.003109 \\ 0.008222 & 0.027371 & 0.014167 & 0.005293 \\ 0.000056 & -0.003109 & -0.005293 & 0.043888 \end{bmatrix}, \tag{48}$$

$$\mathbf{R}^5(0.5,0.5)=\begin{bmatrix} -0.000602 & 0.000035 & 0.000458 & 0.000016 \\ 0.000035 & 0.001571 & 0.001828 & -0.001839 \\ -0.000458 & -0.001828 & 0.004221 & 0.009451 \\ 0.000016 & -0.001839 & -0.009451 & 0.001123 \end{bmatrix}, \tag{49}$$

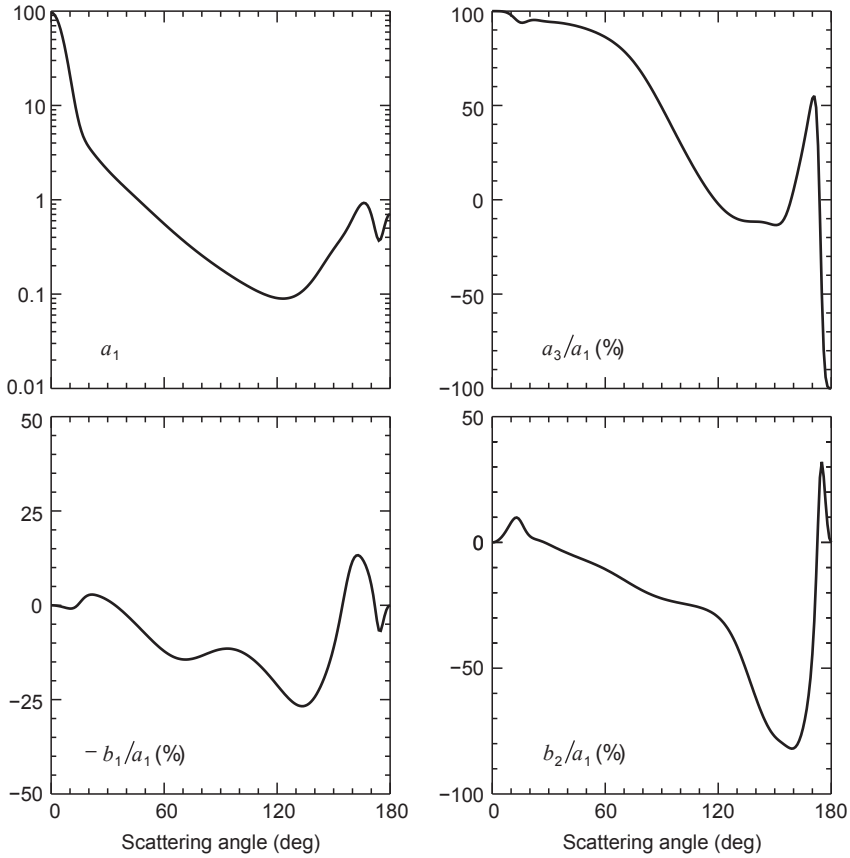

Fig. 3. Nonzero elements of the normalized scattering matrix (2).

$$\mathbf{R}^0(1,1)=\begin{bmatrix} 1.231449 & 0.000000 & 0.000000 & 0.000000 \\ 0.000000 & 0.000000 & 0.000000 & 0.000000 \\ 0.000000 & 0.000000 & 0.000000 & 0.000000 \\ 0.000000 & 0.000000 & 0.000000 & -0.044163 \end{bmatrix}, \tag{50}$$

$$\mathbf{R}^2(1,1)=\begin{bmatrix} 0.000000 & 0.000000 & 0.000000 & 0.000000 \\ 0.000000 & 0.096198 & -0.096198 & 0.000000 \\ 0.000000 & 0.096198 & -0.096198 & 0.000000 \\ 0.000000 & 0.000000 & 0.000000 & 0.000000 \end{bmatrix}. \tag{51}$$

Note that unlike the matrices $\mathbf{R}^m(0.5,0.5)$, all matrices $\mathbf{R}^m(1,1)$ with $m=1$ and $3 \le m \le s_{\max}$ are identically equal to zero, in agreement with the general theoretical analysis in Ref. [19]. The specific structure of the matrices $\mathbf{R}^0(1,1)$ and $\mathbf{R}^2(1,1)$ is also consistent with the general results of Ref. [19]. The matrix $\mathbf{R}^0(0.5,0.5)$ illustrates the block-diagonal structure mentioned in Section 4.5.

Finally, we repeated these radiative-transfer computations for an artificial model of scattering particles having the same expansion coefficients α_i^s and β_i^s listed in Table 1 but a different single-scattering albedo of $\varpi=0.99$. In this case the convergence of iterations for $m=0$ was considerably slower and necessitated a much tighter accuracy requirement EP=1D–8. The resulting number of iterations was 145, as opposed to 48 in the case of conservative scattering ($\varpi=1$). Again, we have verified that the above input parameters guaranteed the accuracy of the resulting benchmark numbers given below:

$$\mathbf{R}^0(0.5,0.5)=\begin{bmatrix} 0.767075 & -0.004616 & 0.000000 & 0.000000 \\ -0.004616 & 0.252512 & 0.000000 & 0.000000 \\ 0.000000 & 0.000000 & 0.141616 & 0.031497 \\ 0.000000 & 0.000000 & -0.031497 & 0.198323 \end{bmatrix}, \tag{52}$$

$$\mathbf{R}^1(0.5,0.5)=\begin{bmatrix} 0.038001 & 0.007563 & -0.013515 & -0.000032 \\ 0.007563 & 0.043512 & 0.033342 & -0.018529 \\ 0.013515 & -0.033342 & 0.157251 & -0.031629 \\ -0.000032 & -0.018529 & 0.031629 & 0.110366 \end{bmatrix}, \tag{53}$$

$$\mathbf{R}^2(0.5,0.5)=\begin{bmatrix} 0.084991 & 0.010966 & -0.007946 & 0.000052 \\ 0.010966 & 0.089781 & -0.026216 & -0.002973 \\ 0.007946 & 0.026216 & 0.014157 & 0.005363 \\ 0.000052 & -0.002973 & -0.005363 & 0.042681 \end{bmatrix}, \tag{54}$$

$$\mathbf{R}^5(0.5,0.5)=\begin{bmatrix} -0.000583 & 0.000034 & 0.000451 & 0.000016 \\ 0.000034 & 0.001529 & 0.001800 & -0.001819 \\ -0.000451 & -0.001800 & 0.004153 & 0.009300 \\ 0.000016 & -0.001819 & -0.009300 & 0.001130 \end{bmatrix}, \tag{55}$$

$$\mathbf{R}^0(1,1)=\begin{bmatrix}0.717801 & 0.000000 & 0.000000 & 0.000000\\ 0.000000 & 0.000000 & 0.000000 & 0.000000\\ 0.000000 & 0.000000 & 0.000000 & 0.000000\\ 0.000000 & 0.000000 & 0.000000 & -0.047557\end{bmatrix}, \tag{56}$$

$$\mathbf{R}^2(1,1)=\begin{bmatrix}0.000000 & 0.000000 & 0.000000 & 0.000000\\ 0.000000 & 0.092979 & -0.092979 & 0.000000\\ 0.000000 & 0.092979 & -0.092979 & 0.000000\\ 0.000000 & 0.000000 & 0.000000 & 0.000000\end{bmatrix}. \tag{57}$$

All digits in Eqs. (52)–(57) have been confirmed by using the completely unrelated adding/doubling program described in Refs. [18,33]. This makes the set of numbers in Eqs. (52)–(57) an objective program-independent benchmark.

6. Concluding remarks

The research summarized in this paper was inspired by Refs. [17,18,26–28,30,34–38] and serves to implement the original ideas proposed therein in the form of an actual publicly available numerical tool. Admittedly, the FORTRAN program pbrf.f is not a universal solver of the vector radiative transfer equation since it can be applied only to optically very thick (semi-infinite) homogeneous layers and does not yield the internal radiation field. However, it is believed to be highly accurate and efficient as well as user friendly. It can be used as a stand-alone tool or in combination with other computer solvers of the vector radiative transfer equation such as the adding/doubling and invariant-imbedding techniques [18,29,32]. Given the rapidly growing interest in polarimetric optical characterization, it is expected that the numerical tool described in this paper will find a good number of practical applications.

For example, the program pbrf.f can be used to compute the reflection matrix of the optically thick ocean interior, and then this matrix can enter the adding solution of the vector radiative transfer equation for the entire ocean–atmosphere system (e.g., [39]). It can also be used to compute the polarized reflectance of optically thick natural or artificial particulate surfaces such as various technical powders as well as snow, soil, and planetary regolith surfaces (e.g., [40–45]). In this case the effects of packing density, coherent backscattering, and macroscopic surface roughness may need to be appropriately accounted for, depending on the actual micro- and macro-physical characteristics of the particulate surface (e.g., [3,13,46–48]). The simplest first-order correction for the packing density effects could be based on the static structure factor approach [49,50]. In the case of an absorbing host medium (e.g., water at near-infrared and infrared wavelengths), the nonlinear integral equation (5) and the program pbrf.f need to be modified according to the microphysical approach developed in Refs. [51–53].

Although the public-domain computer programs mentioned in Section 4.2 are convenient direct sources of the expansion coefficients entering Eqs. (6)–(11), they may be inapplicable to certain particle morphologies and size ranges. In some cases one should be able to use the core-mantle and invariant-imbedding *T*-matrix programs described in Refs. [54–57]. The elements of the scattering matrix (2) can also be computed using alternative numerical techniques such as, for example, the ray tracing (or geometrical optics) approximation [58–66], the discrete-dipole approximation [67–70], the finite-difference time-domain method [71–73], and the pseudo-spectral time domain method [74,75] (see also Refs. [76–83]). Then the expansion coefficients can be calculated by evaluating numerically the following integrals using a suitable quadrature formula:

$$\alpha_1^s=\left(s+\frac{1}{2}\right)\int_0^\pi \mathrm{d}\Theta\ \sin\Theta a_1(\Theta)d_{00}^s(\Theta), \tag{58}$$

$$\alpha_2^s+\alpha_3^s=\left(s+\frac{1}{2}\right)\int_0^\pi \mathrm{d}\Theta\ \sin\Theta\,[a_2(\Theta)+a_3(\Theta)]d_{22}^s(\Theta), \tag{59}$$

$$\alpha_2^s-\alpha_3^s=\left(s+\frac{1}{2}\right)\int_0^\pi \mathrm{d}\Theta\ \sin\Theta\,[a_2(\Theta)-a_3(\Theta)]d_{2,-2}^s(\Theta), \tag{60}$$

$$\alpha_4^s=\left(s+\frac{1}{2}\right)\int_0^\pi \mathrm{d}\Theta\ \sin\Theta a_4(\Theta)d_{00}^s(\Theta), \tag{61}$$

$$\beta_1^s=-\left(s+\frac{1}{2}\right)\int_0^\pi \mathrm{d}\Theta\ \sin\Theta b_1(\Theta)d_{02}^s(\Theta), \tag{62}$$

$$\beta_2^s=-\left(s+\frac{1}{2}\right)\int_0^\pi \mathrm{d}\Theta\ \sin\Theta b_2(\Theta)d_{02}^s(\Theta) \tag{63}$$

(cf. Ref. [84]). Eqs. (58)–(63) follow from Eqs. (6)–(12) and the orthogonality property of the Wigner *d*-functions [3,16].

Acknowledgments

M.I.M. and J.C. acknowledge support from the NASA ACE Project managed by Hal Maring, Paula Bontempi, and David Starr. J.M.D. was supported by the National Academy of Sciences of Ukraine.

References

[1] Mishchenko MI, Dlugach JM, Yanovitskij EG, Zakharova NT. Bidirectional reflectance of flat, optically thick particulate layers: an efficient radiative transfer solution and applications to snow and soil surfaces. J Quant Spectrosc Radiat Transf 1999;63:409–32.
[2] Mishchenko MI, Zakharova NT. FORTRAN codes for the computation of (polarized) bidirectional reflectance of flat particulate layers and rough surfaces. ⟨http://www.giss.nasa.gov/staff/mmishchenko/brf⟩.
[3] Mishchenko MI, Travis LD, Lacis AA. Multiple scattering of light by particles: radiative transfer and coherent backscattering. Cambridge, UK: Cambridge University Press; 2006.
[4] Mishchenko MI, Travis LD. Capabilities and limitations of a current FORTRAN implementation of the T-matrix method for randomly oriented rotationally symmetric scatterers. J Quant Spectrosc Radiat Transf 1998;60:309–24.
[5] Mayer B, Kylling A. Technical note: the libRadtran software package for radiative transfer calculations – description and examples of use. Atmos Chem Phys 2005;5:1855–77.
[6] Buras R, Mayer B. Efficient unbiased variance reduction techniques for Monte Carlo simulations of radiative transfer in cloudy

atmospheres: the solution. J Quant Spectrosc Radiat Transf 2011;112:434–47.
[7] Mackowski DW, Mishchenko MI. A multiple sphere T-matrix Fortran code for use on parallel computer clusters. J Quant Spectrosc Radiat Transf 2011;112:2182–92.
[8] Yurkin MA, Hoekstra AG. The discrete-dipole-approximation code ADDA: capabilities and known limitations. J Quant Spectrosc Radiat Transf 2011;112:2234–47.
[9] Spurr R, Wang J, Zeng J, Mishchenko MI. Linearized T-matrix and Mie scattering computations. J Quant Spectrosc Radiat Transf 2012;113:425–39.
[10] Kahnert M. The T-matrix code *Tsym* for homogeneous dielectric particles with finite symmetries. J Quant Spectrosc Radiat Transf 2013;123:62–78.
[11] Rozanov VV, Rozanov AV, Kokhanovsky AA, Burrows JP. Radiative transfer through terrestrial atmosphere and ocean: software package SCIATRAN. J Quant Spectrosc Radiat Transf 2014;133:13–71.
[12] Mishchenko MI, Travis LD, Lacis AA. Scattering, absorption, and emission of light by small particles. Cambridge, UK: Cambridge University Press; 2002.
[13] Mishchenko MI. Electromagnetic scattering by particles and particle groups: an introduction. Cambridge, UK: Cambridge University Press; 2014.
[14] Mishchenko MI. Measurement of electromagnetic energy flow through a sparse particulate medium: a perspective. J Quant Spectrosc Radiat Transf 2013;123:122–34.
[15] Hovenier JW, van der Mee C, Domke H. Transfer of polarized light in planetary atmospheres—basic concepts and practical methods. Dordrecht, The Netherlands: Kluwer; 2004.
[16] Varshalovich DA, Moskalev AN, Khersonskii VK. Quantum theory of angular momentum. Singapore: World Scientific; 1988.
[17] de Rooij WA. Reflection and transmission of polarized light by planetary atmospheres. Amsterdam: Free University; 1985 (Ph.D. dissertation).
[18] de Haan JF, Bosma PB, Hovenier JW. The adding method for multiple scattering calculations of polarized light. Astron Astrophys 1987;183:371–91.
[19] Hovenier JW, de Haan JF. Polarized light in planetary atmospheres for perpendicular directions. Astron Astrophys 1985;146:185–91.
[20] Krylov VI. Approximate calculation of integrals. New York: Macmillan; 1962.
[21] Mishchenko MI, Mackowski DW. Light scattering by randomly oriented bispheres. Opt Lett 1994;19:1604–6.
[22] Mackowski DW, Mishchenko MI. Calculation of the T matrix and the scattering matrix for ensembles of spheres. J Opt Soc Am A 1996;13:2266–78.
[23] Mackowski DW. A general superposition solution for electromagnetic scattering by multiple spherical domains of optically active media. J Quant Spectrosc Radiat Transf 2014;133:264–70.
[24] Mishchenko MI, Travis LD, Mackowski DW. *T*-Matrix codes for computing electromagnetic scattering by nonspherical and aggregated particles. 〈http://www.giss.nasa.gov/staff/mmishchenko/t_matrix.html〉.
[25] Kahnert M. T matrix code for scattering by homogeneous particles with discrete symmetries. 〈http://www.rss.chalmers.se/~kahnert/Tsym.html〉.
[26] Hansen JE. Multiple scattering of polarized light in planetary atmospheres. II. Sunlight reflected by terrestrial water clouds. J Atmos Sci 1971;28:1400–26.
[27] Dlugach JM, Yanovitskij EG. The optical properties of Venus and the Jovian planets. II. Methods and results of calculations of the intensity of radiation diffusely reflected from semi-infinite homogeneous atmospheres. Icarus 1974;22:66–81.
[28] De Rooij WA, Domke H. On the nonuniqueness of solutions for nonlinear integral equations in radiative transfer theory. J Quant Spectrosc Radiat Transf 1984;31:285–99.
[29] Mishchenko MI. The fast invariant imbedding method for polarized light: computational aspects and numerical results for Rayleigh scattering. J Quant Spectrosc Radiat Transf 1990;43:163–71.
[30] Chandrasekhar S. Radiative transfer. Oxford: Oxford University Press; 1950.
[31] Hansen JE, Hovenier JW. Interpretation of the polarization of Venus. J Atmos Sci 1974;31:1137–60.
[32] Hansen JE, Travis LD. Light scattering in planetary atmospheres. Space Sci Rev 1974;16:527–610.
[33] Chowdhary J, Cairns B, Waquet F, Knobelspiesse K, Ottaviani M, Redemann J, et al. Sensitivity of multiangle, multispectral polarimetric remote sensing over open oceans to water-leaving radiance: analyses of RSP data acquired during the MILAGRO campaign. Remote Sens Environ 2012;118:284–308.
[34] Ambarzumian VA. Diffuse reflection of light by a foggy medium. Comptes Rendus (Doklady) l'Acad Sci l'URSS 1943;38:229–32.
[35] Kuščer I, Ribarič M. Matrix formalism in the theory of diffusion of light. Opt Acta 1959;6:42–51.
[36] Domke H. The expansion of scattering matrices for an isotropic medium in generalized spherical functions. Astrophys Space Sci 1974;29:379–86.
[37] Siewert CE. On the equation of transfer relevant to the scattering of polarized light. Astrophys J 1981;245:1080–6.
[38] Hovenier JW, van der Mee CVM. Fundamental relationships relevant to the transfer of polarized light in a scattering atmosphere. Astron Astrophys 1983;128:1–16.
[39] Chowdhary J, Cairns B, Mishchenko MI, Hobbs PV, Cota GF, Redemann J, et al. Retrieval of aerosol scattering and absorption properties from photopolarimetric observations over the ocean during the CLAMS experiment. J Atmos Sci 2005;62:1093–117.
[40] Wiscombe WJ, Warren SG. A model for the spectral albedo of snow. I: Pure snow. J Atmos Sci 1980;37:2712–33.
[41] Dozier J. Remote sensing of snow in the visible and near-infrared wavelengths. In: Asrar G, editor. Theory and applications of optical remote sensing. New York: Wiley; 1989. p. 527–47.
[42] Painter TH, Dozier J. Measurements of the hemispherical-directional reflectance of snow at fine spectral and angular resolution. J Geophys Res 2004;109:D18115.
[43] Zhang H, Voss K. Bidirectional reflectance and polarization measurements on packed surfaces of benthic sediments and spherical particles. Opt Express 2009;17:5217–31.
[44] Peltoniemi J, Hakala T, Suomalainen J, Puttonen E. Polarised bidirectional reflectance factor measurements from soil, stones, and snow. J Quant Spectrosc Radiat Transf 2009;110:1940–53.
[45] Goguen JD. Planetary surface photometry and imaging: progress and perspectives. Rep Prog Phys 2014;77:104901.
[46] Lyapustin A, Gatebe CK, Kahn R, Brandt R, Redemann J, Russell P, et al. Analysis of snow bidirectional reflectance from ARCTAS Spring-2008 Campaign. Atmos Chem Phys 2010;10:4359–75.
[47] Tishkovets VP, Petrova EV, Mishchenko MI. Scattering of electromagnetic waves by ensembles of particles and discrete random media. J Quant Spectrosc Radiat Transf 2011;112:2095–127.
[48] Muinonen K, Mishchenko MI, Dlugach JM, Zubko E, Penttilä A, Videen G. Coherent backscattering verified numerically for a finite volume of spherical particles. Astrophys J 2012;760:118.
[49] Mishchenko MI. Asymmetry parameters of the phase function for densely packed scattering grains. J Quant Spectrosc Radiat Transf 1994;52:95–110.
[50] Mishchenko MI, Goldstein D, Chowdhary J, Lompado A. Radiative transfer theory verified by controlled laboratory experiments. Opt Lett 2013;38:3522–5.
[51] Mishchenko MI. Electromagnetic scattering by a fixed finite object embedded in an absorbing medium. Opt Express 2007;15:13188–202.
[52] Mishchenko MI. Multiple scattering by particles embedded in an absorbing medium. 1. Foldy–Lax equations, order-of-scattering expansion, and coherent field. Opt Express 2008;16:2288–301.
[53] Mishchenko MI. Multiple scattering by particles embedded in an absorbing medium. 2. Radiative transfer equation. J Quant Spectrosc Radiat Transf 2008;109:2386–90.
[54] Quirantes A. Light scattering properties of spheroidal coated particles in random orientation. J Quant Spectrosc Radiat Transf 1999;63:263–75.
[55] Bi L, Yang P, Kattawar GW, Mishchenko MI. Efficient implementation of the invariant imbedding T-matrix method and the separation of variables method applied to large nonspherical inhomogeneous particles. J Quant Spectrosc Radiat Transf 2013;116:169–83.
[56] Bi L, Yang P, Kattawar GW, Mishchenko MI. A numerical combination of extended boundary condition method and invariant imbedding method applied to light scattering by large spheroids and cylinders. J Quant Spectrosc Radiat Transf 2013;123:17–22.
[57] Bi L, Yang P. Accurate simulation of the optical properties of atmospheric ice crystals with the invariant imbedding T-matrix method. J Quant Spectrosc Radiat Transf 2014;138:17–35.
[58] Macke A, Mueller J, Raschke E. Scattering properties of atmospheric ice crystals. J Atmos Sci 1996;53:2813–25.
[59] Macke A, Mishchenko MI. Applicability of regular particle shapes in light scattering calculations for atmospheric ice particles. Appl Opt 1996;35:4291–6.
[60] Yang P, Liou KN. Geometric-optics–integral-equation method for light scattering by nonspherical ice crystals. Appl Opt 1996;35:6568–84.
[61] Muinonen K, Nousiainen T, Fast P, Lumme K, Peltoniemi JI. Light scattering by Gaussian random particles: ray optics approximation. J Quant Spectrosc Radiat Transf 1996;55:577–601.

[62] Liou KN, Takano Y, Yang P. Light scattering and radiative transfer in ice crystal clouds: applications to climate research. In: Mishchenko MI, Hovenier JW, Travis LD, editors. Light scattering by nonspherical particles: theory, measurements, and applications. San Diego: Academic Press; 2000. p. 417–49.
[63] Macke A. Monte Carlo calculations of light scattering by large particles with multiple internal inclusions. In: Mishchenko MI, Hovenier JW, Travis LD, editors. Light scattering by nonspherical particles: theory, measurements, and applications. San Diego: Academic Press; 2000. p. 309–22.
[64] Yang P, Liou KN. Light scattering and absorption by nonspherical ice crystals. Light Scatt Rev 2006;1:31–71.
[65] Bi L, Yang P. Physical-geometric optics hybrid methods for computing the scattering and absorption properties of ice crystals and dust aerosols. Light Scatt Rev 2013;8:69–114.
[66] Borovoi A, Konoshonkin A, Kustova N. The physical-optics approximation and its application to light backscattering by hexagonal ice crystals. J Quant Spectrosc Radiat Transf 2014;146:181–9.
[67] Draine BT, Flatau PJ. Discrete dipole approximation for scattering calculations. J Opt Soc Am A 1994;11:1491–9.
[68] Draine BT. The discrete dipole approximation for light scattering by irregular targets. In: Mishchenko MI, Hovenier JW, Travis LD, editors. Light scattering by nonspherical particles: theory, measurements, and applications. San Diego: Academic Press; 2000. p. 131–45.
[69] Yurkin MA, Hoekstra AG. The discrete dipole approximation: an overview and recent developments. J Quant Spectrosc Radiat Transf 2007;106:558–89.
[70] Yurkin MA, Hoekstra AG. The discrete-dipole-approximation code ADDA: capabilities and known limitations. J Quant Spectrosc Radiat Transf 2011;112:2234–47.
[71] Yang P, Liou KN. Finite difference time domain method for light scattering by nonspherical and inhomogeneous particles. In: Mishchenko MI, Hovenier JW, Travis LD, editors. Light scattering by nonspherical particles: theory, measurements, and applications. San Diego: Academic Press; 2000. p. 173–221.
[72] Taflove A, Hagness SC. Computational electrodynamics: the finite-difference time-domain method. Boston: Artech House; 2005.
[73] Inan US, Marshall RA. Numerical electromagnetics: the FDTD method. Cambridge, UK: Cambridge University Press; 2011.
[74] Panetta RL, Liu C, Yang P. A pseudo-spectral time domain method for light scattering computation. Light Scatt Rev 2013;8:139–88.
[75] Liu C, Panetta RL, Yang P. Inhomogeneity structure and the applicability of effective medium approximations in calculating light scattering by inhomogeneous particles. J Quant Spectrosc Radiat Transf 2014;146:331–48.
[76] Volakis JL, Chatterjee A, Kempel LC. Finite element method for electromagnetics. New York: IEEE Press; 1998.
[77] Wriedt T, editor. Generalized multipole techniques for electromagnetic and light scattering. Amsterdam: Elsevier; 1999.
[78] Jin J. The finite element method in electromagnetics. New York: Wiley; 2002.
[79] Kahnert FM. Numerical methods in electromagnetic scattering theory. J Quant Spectrosc Radiat Transf 2003;79–80:775–824.
[80] Doicu A, Wriedt T, Eremin YuA. Light scattering by systems of particles. Null-field method with discrete sources: theory and programs. Berlin: Springer; 2006.
[81] Farafonov VG, Il'in VB. Single light scattering: computational methods. Light Scatt Rev 2006;1:125–77.
[82] Quinten M. Optical properties of nanoparticle systems. Weinheim, Germany: Wiley-VCH; 2011.
[83] Rother T, Kahnert M. Electromagnetic wave scattering on nonspherical particles. Basic methodology and simulations. Berlin: Springer; 2014.
[84] Mishchenko MI, Macke A. Incorporation of physical optics effects and computations of the Legendre expansion for ray-tracing phase functions involving delta-function transmission. J Geophys Res 1998;103:1799–805.